

Precipitation Behavior of Thermo-Mechanically Treated $\text{Ti}_{50}\text{Ni}_{20}\text{Au}_{20}\text{Cu}_{10}$ High-Temperature Shape-Memory Alloy

Saif Haider Kayani^{1,3} · M. Imran Khan¹ · Fazal Ahmad Khalid^{1,2} · Hee Young Kim⁴ · Shuichi Miyazaki^{4,5}

Published online: 21 December 2015
© ASM International 2015

Abstract In the present work, precipitation behavior of TiNiAuCu-based high-temperature shape-memory alloys is studied. Two alloys with compositions $\text{Ti}_{50}\text{Ni}_{30}\text{Au}_{20}$ and $\text{Ti}_{50}\text{Ni}_{20}\text{Au}_{20}\text{Cu}_{10}$ were prepared. After 30 % cold rolling, both alloys were then annealed at different temperatures. Formation of Cu-rich TiAuCu and Ti-rich Ti_3Au precipitates was observed in $\text{Ti}_{50}\text{Ni}_{20}\text{Au}_{20}\text{Cu}_{10}$ alloy when annealed at different temperatures after cold deformation. It was noticed that prior cold deformation has significant effect on the precipitation behavior. A similar kind of precipitation behavior has been previously reported in TiNiPdCu alloys. Both TiAuCu and Ti_3Au type precipitates were found to be deficient in Ni content which causes

an increase in Ni content of the matrix and a small decrease in transformation temperatures of the $\text{Ti}_{50}\text{Ni}_{20}\text{Au}_{20}\text{Cu}_{10}$ alloy.

Keywords High-temperature shape-memory alloy · TiNiAu · Cold deformation · Precipitation hardening

Introduction

Interests in high-temperature shape-memory alloys (HTSMAs) have been significantly increased mainly due to their potential use in new engineering applications especially related to aerospace, automotive, and robotics industry [1, 2]. The usage of binary TiNi alloy is limited to those applications where temperature is below 373 K, mainly due to its low-transformation temperatures. It has been reported that ternary additions such as Pt, Au, Pd, Hf, and Zr increase the transformation temperatures of TiNi-based shape-memory alloys [3–6].

TiNiPd- and TiNiPt-based HTSMAs have been extensively investigated, since their discovery, but very little literature is available on TiNiAu-based HTSMAs [7, 8]. TiNiPd system gives better shape-memory properties but exhibits relatively lower transformation temperatures in comparison to TiNiPt and TiNiAu systems. Relatively very high transformation temperatures have been reported for TiNiPt system, but its shape-memory properties are quite poor. The TiNiAu ternary system gives a balanced compromise between the transformation temperatures and shape-memory properties. The TiAu-based binary system has the highest transformation temperatures after the TiPt-based binary system [9, 10]. Wayman and Wu reported the M_s temperatures of about 883 and 713 K for $\text{Ti}_{50}\text{Au}_{50}$ and $\text{Ti}_{50}\text{Ni}_{10}\text{Au}_{40}$ alloys, respectively, with stable SME [11].

This article is an invited paper selected from presentations at the International Conference on High-Temperature Shape Memory Alloys 2015, held May 5–8, 2015, in Wildbad Kreuth Educational Centre in Kreuth, Bavaria, Germany, and has been expanded from the original presentation.

✉ Saif Haider Kayani
saifkayani@kims.re.kr

✉ M. Imran Khan
imran961137@hotmail.com

¹ Ghulam Ishaq Khan (GIK) Institute of Engineering Sciences and Technology, Topi, District Swabi, Khyber Pakhtunkhwa 23640, Pakistan

² University of Engineering and Technology, Lahore, Pakistan

³ Korea Institute of Materials Science, 797 Changwondaero, Seongsangu, Changwon, Gyeongnam 642-831, Republic of Korea

⁴ Division of Materials Science, University of Tsukuba, Tsukuba, Ibaraki 305-8573, Japan

⁵ Foundation for Advancement of International Science, 3-24-16 Kasuga, Tsukuba, Ibaraki 305-0821, Japan

The same research group reported the M_s temperatures of about 293 and 282 K for $Ti_{50}Ni_{40}Au_{10}$ and $Ti_{50}Ni_{45}Au_5$ alloys, respectively [12, 13]. It has also been reported that transformation temperatures decrease in $Ti_{50}Ni_{50-x}Au_x$ alloys with lowering Au content, because Au has an affinity to sit on Ni lattice sites within ordered B2 phase just like Pt and Pd in TiNiPt- and TiNiPd-based HTSMAs, respectively. The parent phase of TiAu binary system also has an ordered B2 (CsCl type) crystal structure at near equiatomic concentration [14].

Recently, Butler has reported the formation of Ti-, Au-, and Ni-based precipitates in $Ti_{50}Ni_{25}Au_{25}$ alloy as a result of aging at different temperatures [15]. These precipitates suppressed the martensitic transformation due to the formation of Ni-rich matrix in $Ti_{50}Ni_{25}Au_{25}$ in addition to precipitation-hardening effect. Researches showed that transformation temperature and cyclic stability of TiNi-based HTSMAs can be improved by quaternary additions, strain hardening, and precipitation strengthening. Khan et al. [16–19] have recently reported the formation of nanoscale precipitates in $Ti_{50}Ni_{25-x}Pd_{25}Cu_x$ alloys as an effect of annealing after cold deformation, and this topic was reviewed in Ref. [20]. These precipitates significantly increased the cyclic stability and creep resistance of TiNiPdCu-based HTSMAs. Both Cu addition and annealing after cold rolling play important roles in the formation of these precipitates. TiNiAu system is similar to TiNiPd system and it is expected that a similar kind of nanoscale precipitation behavior could be present in these alloys that could improve the cyclic stability of TiNiAu-based HTSMAs as well. In the present study, the effects of Cu addition and annealing after cold deformation on the microstructure and transformation temperatures of TiNiAu-based HTSMAs were investigated in order to confirm the presence of a similar kind of precipitation behavior in these alloys.

Experimental

$Ti_{50}Ni_{30}Au_{20}$ and $Ti_{50}Ni_{20}Au_{20}Cu_{10}$ alloys were prepared by Ar-arc melting. Hereafter, the alloys are referred to as 0Cu and 10Cu according to their Cu contents. Each alloy button was flipped and re-melted five times in order to maximize the homogeneity. Both alloys were then homogenized at 1323 K for 9 ks in argon gas atmosphere. The homogenized samples were cold rolled up to 30 %. Cold-rolled (CR) samples were annealed at 773, 873, and 973 K for 3.6 ks in argon atmosphere. Hereafter, these samples are referred to as annealed samples with designations A5, A6, and A7, respectively. The solution treatment of some cold-rolled samples of both alloys was also

done at 1323 K for 3.6 ks in argon atmosphere mainly for comparison purposes.

Samples for scanning electron microscope (SEM), X-ray diffraction (XRD), differential scanning calorimetry (DSC), and microhardness were cut using an electro discharge machine (EDM). Microstructural analysis was done using a MIRA3 TESCAN SEM. Imaging was carried out in backscattered (BSE) mode, in order to improve the atomic number (Z) contrast of the phases present. Energy-dispersive X-ray spectroscopy (EDS) analysis was performed to determine the composition of various phases using QUANTAX EDS Bruker with an accelerating voltage of 20 kV. Room temperature X-ray diffraction measurements were used to perform phase analysis using Philips X-ray diffractometer (model PW 3710). DSC was used to determine the transformation temperatures of the samples with heating and cooling rates of 10 K/min. Microhardness (H_v) values of all the samples were taken using TUKON microhardness tester (model-300) under a load of 500 g.

Results

Microstructural Analysis

Backscattered SEM image of the 10Cu alloy annealed at different temperatures after cold deformation is shown in Fig. 1a–c.

Microstructure of 10Cu alloy annealed at 773 K revealed that precipitation started after annealing at 773 K as shown in Fig. 1a. It was observed that size of precipitates was increased and their density decreased after annealing at 873 and 973 K (Fig. 1b, c). In backscattered scanning electron microscopy (BS-SEM) images of 10Cu alloys, annealed at different temperatures after cold rolling, round/elliptical shaped precipitates were observed which were surrounded by darker contrast regions. In BS-SEM images, darker contrast region usually indicates the presence of lighter elements and brighter region indicates the presence of heavier elements. Atomic number of Ti is 22 suggesting that it is lighter than Au, Ni, and Cu, so these darker and brighter regions must be Ti-rich and Ti-lean in composition, respectively. The compositional analysis of the precipitates is explained in the next section.

Figure 1d shows the BS-SEM image of 10Cu alloy which was solution treated at 1323 K. No precipitate was observed to form in the solution-treated samples, and a very fine martensitic structure can be seen in the microstructure.

The 0Cu alloy did not show any noticeable change in the microstructure upon annealing after 30 % cold deformation and showed only the twinned structure of orthorhombic

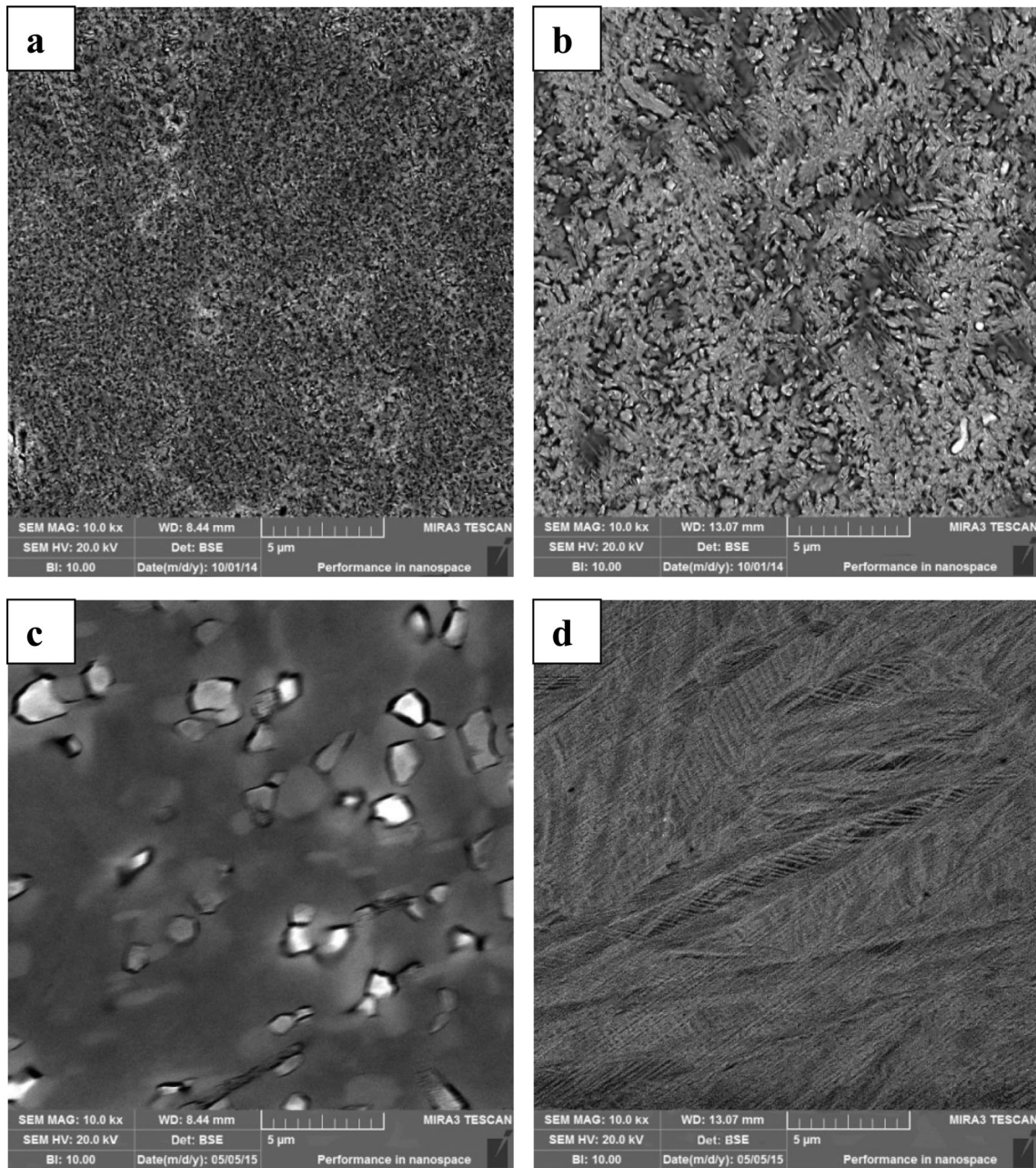


Fig. 1 BSE SEM image of 10Cu alloy. **a** Annealed at 773 K, **b** annealed at 873 K, **c** annealed at 973 K, and **d** solution treated

B19 martensite. The microstructural features were exactly the same as shown in case of solution-treated 10Cu alloy sample as shown in Fig. 1d. That is why the images of 0Cu alloy samples are not shown here.

Compositional Analysis

To determine the chemical composition of both dark and bright precipitates, EDS spot analysis was used. 10Cu alloy sample, annealed at 973 K, was chosen to determine the

composition mainly due to a relatively larger size of precipitates in this sample. EDS chemical spot analysis spectrum is shown in Fig. 2. The quantitative values of the EDS spot chemical composition analysis are shown in Table 1. EDS spot analysis clearly showed that the brighter regions were lean in Ti and rich in Cu as compared to the darker regions. The EDS results also confirmed that the dark regions were Ti-rich regions. Both regions were lean in Ni as compared to the intended composition of the matrix.

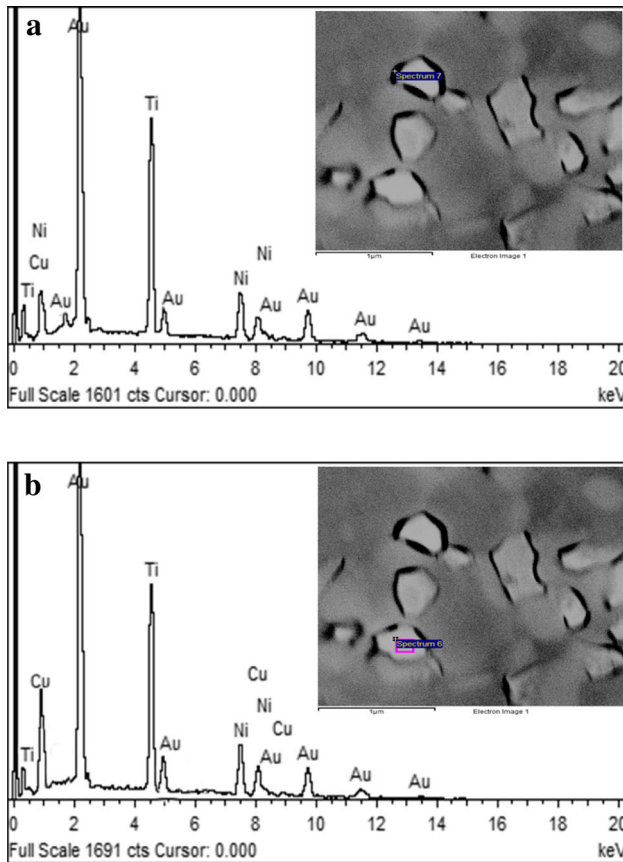


Fig. 2 EDS spot chemical composition analysis spectrum of **a** black precipitates and **b** white precipitates formed in 10Cu A7 sample

Phase Analysis

Figure 3a, b show XRD profile of 0Cu and 10Cu alloys. In cold-rolled 0Cu and 10Cu alloys, each XRD profile showed the presence of a wide peak of (111) B19 martensite. This broadening of the strong (111) B19 peak is due to the presence of residual strains induced by the deformation-induced defects. In case of 0Cu alloy annealed at 773 K, a sharp peak of (111) B19 and other B19 peaks from (020) and (002) were observed that indicated the removal of cold deformation-induced defects because of stress relieving process that took place during annealing. XRD profile of 10Cu alloy annealed at 773 K was significantly different from 0Cu alloy. Along with the peaks (111) (020), (002) from B19 martensite variants, a B2 parent phase peak and Ti_3Au peaks from (200), (210), (321), and (400) were detected. A strong peak at 2θ of 44.568° could not be

identified using JCPDS standard database. EDS analysis indicated the strong presence of $TiAuCu$ -type phase, suggesting that this unknown peak could be of $TiAuCu$ -type precipitates. In case of 0Cu alloy, annealed at 873 and 973 K, sharp XRD peaks of B19 martensite were observed which were very similar to that of solution-treated 0Cu alloy. However, XRD profiles of 10Cu alloy annealed at 873 K resulted in increase of B19 martensite peaks at the expense of B2 peaks. After annealing at 973 K (111), (020), and (002) B19 martensite peaks and (200), (321), and (400) Ti_3Au peaks became stronger. This indicated that the precipitates density was increased with the increasing annealing temperature. XRD profile of solution-treated 10Cu alloy was similar to that of solution-treated 0Cu alloy and only showed the presence of B19 martensite peaks.

This observation confirmed that cold deformation before annealing strongly promoted the formation of Ti_3Au and $TiAuCu$ -type precipitates in $Ti_{50}Ni_{20}Au_{20}Cu_{10}$ alloy. This precipitation behavior was not observed in 0Cu alloy. So, it was expected that deformation-induced defects acted as heterogeneous nucleation sites for the nucleation of $TiAuCu$ -type precipitates which in turn promoted the formation of Ti_3Au type precipitates. Recently, similar kind of Ti-rich and Cu-rich precipitates have been reported in $TiNiPdCu$ alloys revealing that annealing after cold rolling promoted the formation of precipitates only in $TiNiPd$ alloys with quaternary additions of Cu, but neither kind of precipitation was observed in alloys without Cu addition [16]. This previously published observation is consistent with the present work.

Previously, it was reported that the addition of Cu increased the lattice parameters of B19 martensite in $TiNiPd$ system [7, 21]. In order to confirm the similar effect in case of $TiNiAuCu$ alloys, lattice parameters of solution-treated 0Cu and 10Cu alloys and 10Cu alloy annealed at 973 K were calculated, and the results are given in Table 2. It can be seen that the solution-treated 0Cu alloy have smaller values of a, b, and c. Lattice parameters of solution-treated 10Cu alloy are higher than that of 0Cu alloy, implying that addition of 10 at.% Cu increased the lattice parameters. But for 10Cu alloy annealed at 973 K, lattice parameters were almost the same as 0Cu alloy. This can be explained by the fact that the formation of $TiAuCu$ -type precipitates, upon annealing, actually decreases the overall contents of Cu in the matrix which ultimately decreases the lattice parameters.

Table 1 EDS spot chemical composition analysis of black and white precipitates formed in 10Cu-A7 sample

S. no	Analysis region	Ti (at.%)	Ni (at.%)	Au (at.%)	Cu (at.%)
1	Black precipitates	47.56	17.78	25.77	8.89
2	White precipitates	36.57	15.78	25.66	21.99

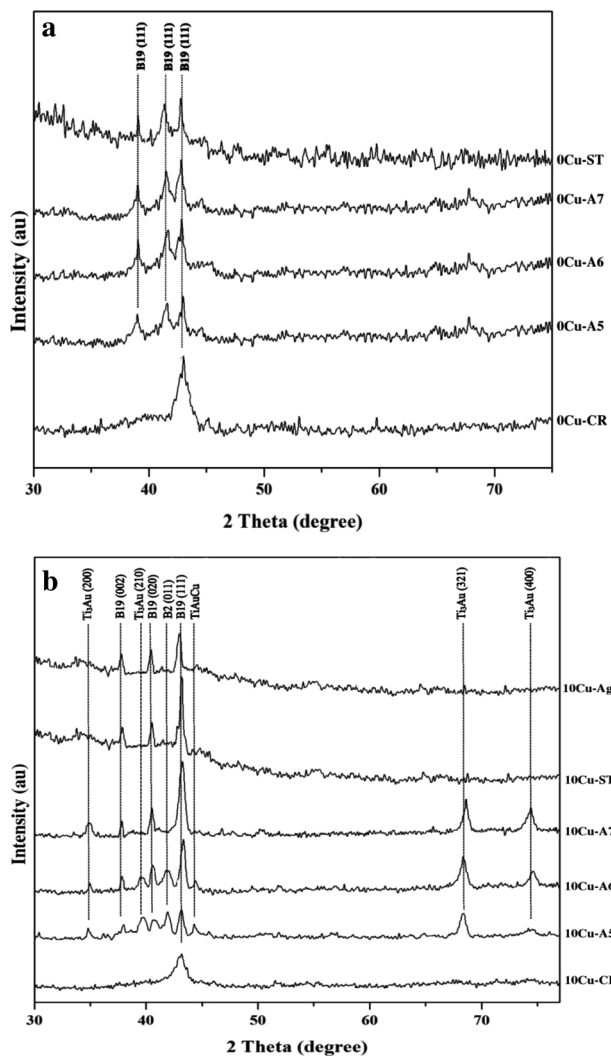


Fig. 3 XRD profiles of **a** 0Cu and **b** 10Cu alloys after 30 % cold deformation, solution treatment, and annealing at various temperatures

Table 2 Comparison of lattice parameters value in 0Cu solution treated, 10Cu solution treated, and 10Cu annealed at 973 K

Sample I.D	a (Å)	b (Å)	c (Å)
0Cu-ST	1.71	1.55	2.73
10Cu-ST	2.11	1.56	3.90
10Cu-A7	1.79	1.55	2.75

Differential Scanning Calorimetry (DSC) Analysis

Figure 4a shows the DSC curves of 0Cu alloy after 30 % cold rolling, solution treatment, and annealing at various temperatures after 30 % cold rolling. Very small and broad peaks were observed in 30 % cold-rolled 0Cu alloy,

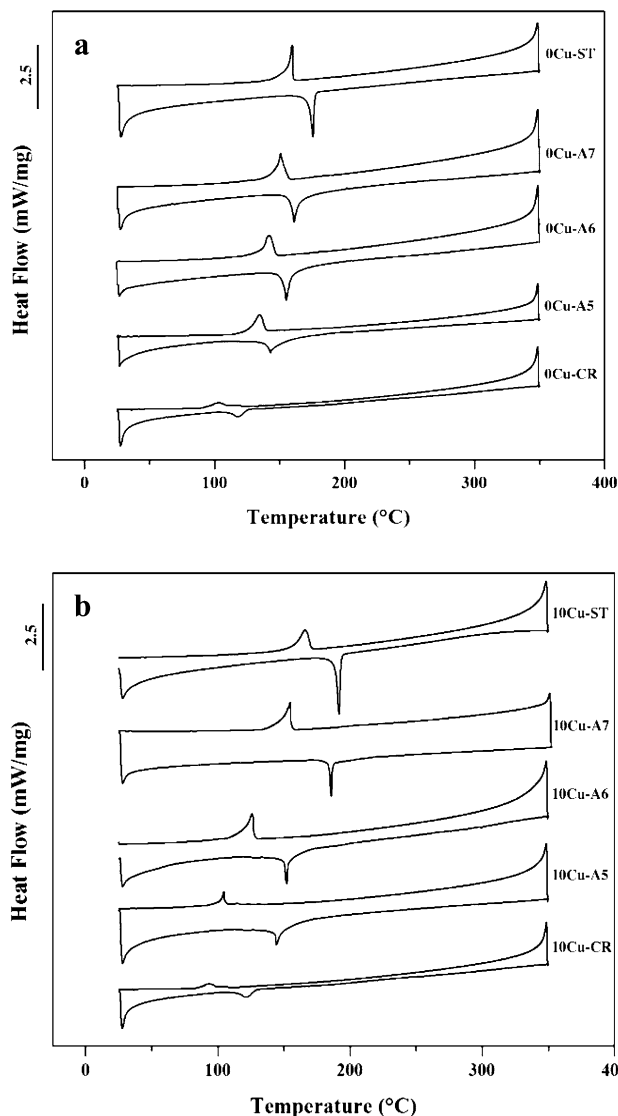


Fig. 4 DSC curves of **a** 0Cu and **b** 10Cu alloys after 30 % cold rolling, solution treatment, and annealing at various temperatures

suggesting that the martensitic transformation is suppressed due to the presence of internal stresses developed after cold rolling. Well-developed but small transformation peaks were observed in 0Cu alloy after annealing at 773 K. Figure 5a shows the transformation temperatures of 0Cu alloy in cold-rolled, solution-treated and annealed conditions. Samples, annealed at higher temperatures such as 873 K and 973 K showed almost similar transformation temperatures compared to that of solution-treated sample, i.e., for solution-treated alloys $M_s = 437$ K and $A_f = 455$ K. This showed that annealing after cold deformation resulted in the removal of most of the defects by recovery and recrystallization process. This behavior was also confirmed by the XRD profiles of annealed samples of 0Cu alloy.

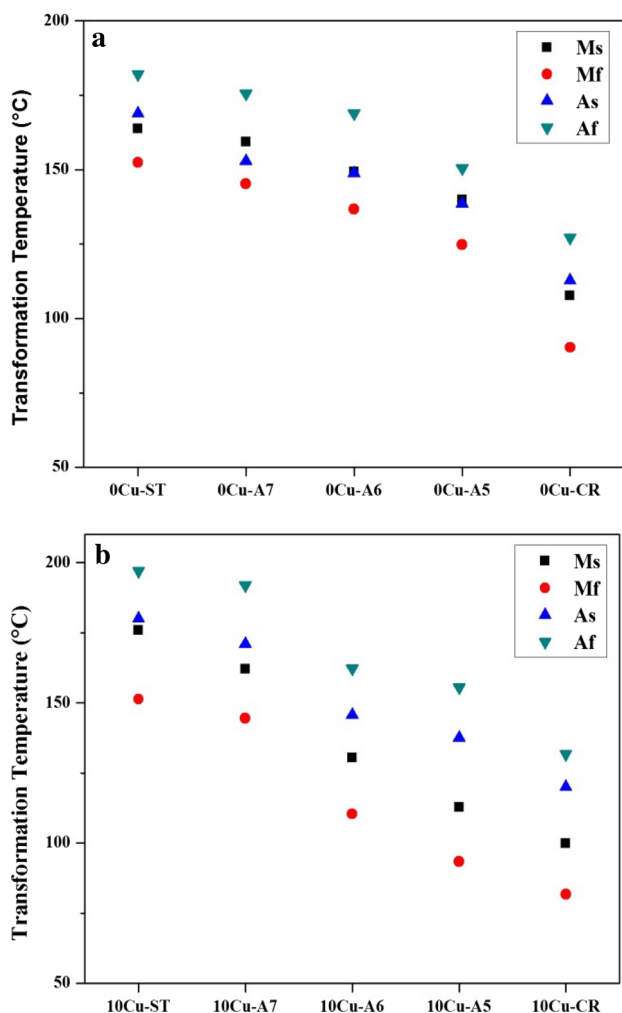


Fig. 5 Evolution of transformation temperatures of **a** 0Cu and **b** 10Cu alloy after 30 % cold rolling, solution treatment, and annealing at various temperatures

Figure 4b shows the DSC curves of 10Cu alloy after solution treatment, 30 % cold rolling, and annealing at various temperatures. Cold-rolled 10Cu alloy showed lower transformation temperatures and relatively broad peaks, mainly due to the introduction of large number of defects which suppressed the martensitic transformation. Smaller but sharper forward and reverse martensitic transformation peaks were observed in case of 773 K annealed 10Cu alloy. 10Cu alloys annealed at higher temperatures showed slight increase in transformation temperatures and sharper transformation peaks. Figure 5b shows transformation temperatures of solution-treated and annealed 10Cu alloy samples. Solution-treated 10Cu sample showed higher transformation temperature as compared to that of solution-treated 0Cu sample. 10Cu alloy annealed at 773 K after 30 % cold deformation showed lower transformation temperatures as compared to that of solution-treated 10Cu alloy. Annealing at 873 K slightly

increased the transformation temperatures. 10Cu alloy annealed at 973 K showed almost similar transformation temperatures as compared to that of solution-treated 10Cu sample.

The decrease in transformation temperatures of 10Cu samples, annealed after cold deformation could be attributed to the compositional changes occurred due to the precipitation of Ti-rich and Cu-rich precipitates. XRD profiles of the annealed 10Cu samples also indicated the formation of B2 parent phase along with the precipitates and B19 martensite. EDS spot analysis, given in Table 1, showed that both precipitates have smaller Ni contents. This suggests that Ni content in the matrix must be high and this might be a strong reason for the decrease in transformation temperatures. X-ray mapping of 973 K annealed sample in Fig. 6 showed a high density of small white spots in matrix indicating high Ni content in the matrix while low Ni content in precipitates.

Microhardness

Figure 7 shows the microhardness values of annealed 0Cu and 10Cu alloys. Figure 7 also shows the hardness values of solution-treated alloys for comparison purpose. 30 % cold-deformed, solution-treated and annealed 10Cu alloys showed higher hardness value in comparison to that of 0Cu alloy. This difference in the hardness of 0Cu and 10Cu alloys is because of solid solution strengthening effect of Cu in TiNiAu alloys. Khan et al. also reported this effect of Cu in TiNiPd alloys [7]. 0Cu cold-deformed sample revealed a high hardness value than 0Cu-annealed alloys; this is because of work-hardening effect. After annealing the cold-rolled samples at 773–973 K, hardness value decreased. This drop in hardness value is attributed to the removal of cold deformation-induced defects by recovery and recrystallization mechanism during annealing. But hardness values revealed a different trend in case of annealed 10Cu alloy samples. Hardness values started to increase in 773 K annealed sample, and it further increased up to 680H_v in case of 873 K annealed sample. This increase in hardness was due to the formation of very fine, homogenous, and highly dense precipitates which were formed in 10Cu alloy after annealing at different temperatures. 973 K annealed 10Cu alloy showed a significant decrease in the hardness values mainly due the increase in the size of precipitates and decrease in their density.

Conclusions

In this research work, precipitation behavior of annealed Ti₅₀Ni₂₀Au₂₀Cu₁₀ alloy was studied. Present study confirms the presence of a defect-assisted precipitation

Fig. 6 X-ray mapping of 10Cu alloy annealed at 973 K showing distribution of alloying elements

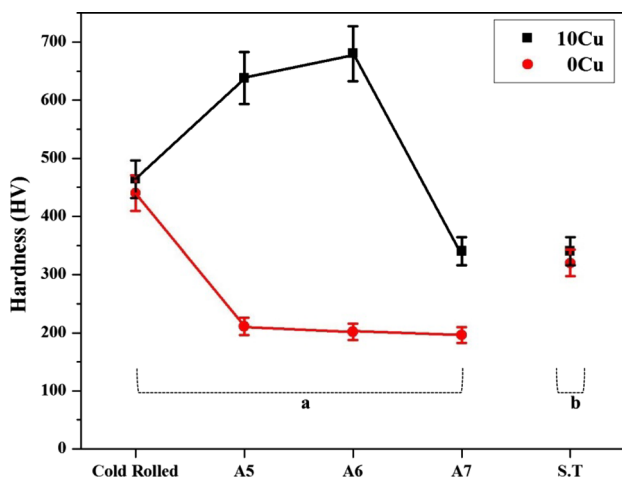


Fig. 7 Microhardness of 0Cu and 10Cu alloys **a** 30 % cold rolled followed by annealing at various temperatures and **b** solution treated at 1323 K

mechanism in TiNiAuCu-based HTSMAs that are similar to the precipitation mechanism previously observed in TiNiPdCu-based HTSMAs. Major findings of the current study are given below:

- (1) An expected, precipitation behavior was found in annealed TiNiAuCu alloys and high densities of TiNiAu and Ti_3Au type precipitates were observed in these alloys.
- (2) It is confirmed that TiAuCu and Ti_3Au type precipitates are formed in the cold rolled and subsequently annealed TiNiAuCu-based HTSMAs.
- (3) Both types of precipitates were found to be lean in Ni content because of low solubility of Ni in both precipitates.
- (4) The formation of high densities of two types of Ni lean precipitates significantly increased the Ni content of the matrix which significantly suppressed the transformation temperatures.

- (5) These precipitates were found to be stable up to about 873 K and effective in suppressing the recovery/recrystallization type processes, which are the real threat to high-temperature stability of HTSMAs.

Acknowledgments This work was supported by Ghulam Ishaq Khan (GIK) Institute of Engineering Sciences and Technology, Topi, Pakistan.

References

1. Mohd Jani J, Leary M, Subic A, Subic MA Gibson (2014) A review of shape memory alloy research, applications and opportunities. *Mater Des* 56:1078–1113
2. Padula S, Bigelow G, Noebe R, Gaydos D, Garg A (2006) Challenges and progress in the development of high-temperature shape memory alloys based on NiTiX compositions for high-force actuator applications. NASA Glenn Res, Cent
3. Ma J, Karaman I, Noebe RD (1999) High temperature shape memory alloys. *Int Mater Rev* 55:257–315
4. Benafan O, Noebe RD, Padula SA, Vaidyanathan R (2012) Microstructural response during isothermal and isobaric loading of a precipitation-strengthened Ni-29.7Ti-20Hf high-temperature shape memory alloy. *Metall Mater Trans A* 43:4539–4552
5. Van Humbeeck J (2012) Shape memory alloys with high transformation temperatures. *Mater Res Bull* 47:2966–2968
6. Otsuka K, Ren X (2005) Physical metallurgy of Ti–Ni-based shape memory alloys. *Prog Mater Sci* 50:511–678
7. Khan IM, Kim HY, Nam TH, Miyazaki S (2013) Effect of Cu addition on the high temperature shape memory properties of $\text{Ti}_{50}\text{Ni}_{25}\text{Pd}_{25}$ alloy. *J Alloys Compd* 577:383–387
8. Soboyejo WO, Srivatsan TS (2006) Advanced structural materials properties, design optimization and applications. CRC Press, Boca Raton
9. Rios O, Noebe R, Biles T, Garg A, Palczar A, Scheiman D, Seifert HJ, Kaufman M (2005) Characterization of ternary NiTiPt high-temperature shape memory alloys. *SPIE Proc* 5761:376–387
10. Donkersloot HC, Van Vucht JHN (1970) Martensitic transformation in gold-titanium, palladium-titanium and platinum-titanium alloys near the equiatomic composition. *J Less Common Met* 20:83–91

11. Wu SK, Wayman CM (1987) Martensitic transformations and the shape memory effect in $\text{Ti}_{50}\text{Ni}_{10}\text{Au}_{40}$ and $\text{Ti}_{50}\text{Au}_{50}$ alloys. *Metallography* 20:359–376
12. Wu SK, Wayman CM (1987) Transmission electron microscopy studies of the martensitic transformation in a $\text{Ti}_{50}\text{Ni}_{45}\text{Au}_5$ Alloy. *Mater Sci Eng* 96:295–302
13. Wu SK, Wayman CM (1987) TEM studies of the martensitic transformation in a $\text{Ti}_{50}\text{Ni}_{40}\text{Au}_{10}$ alloy. *Scr Metall* 21:83–88
14. Vermaut P, Declairieux C, Ochin P, Kolomytsev V, Pasko A, Monastyrsky G (2013) Martensitic transformation and shape memory effect at very high temperatures in HfPd, and TiAu intermetallic compounds. *J Alloys Compd.* 577:S388–S392
15. Butler T (2013) Structure and properties of Ti-Ni-Au shape memory alloys. The University of Alabama, Tuscaloosa
16. Imran Khan M, Kim HY, Kim TH, Miyazaki S (2012) Formation of nanoscaled precipitates and their effects on the high-temperature shape-memory characteristics of a $\text{Ti}_{50}\text{Ni}_{15}\text{Pd}_{25}\text{Cu}_{10}$ alloy. *Acta Mater* 60:5900–5913
17. Khan MI, Young H, Namigata Y, Nam T (2013) Combined effects of work hardening and precipitation strengthening on the cyclic stability of TiNiPdCu-based high-temperature shape memory alloys. *Acta Mater* 61:4797–4810
18. Khan MI, Kim HY, Khalid FA, Miyazaki S (2014) Effect of cold rolling ratio on the nanoscale precipitation behavior of TiNiPdCu based high temperature shape memory alloys. *J Alloys Compd* 599:212–218
19. Imahashi M, Khan MI, Kim HY, Miyazaki S (2014) The effect of Pd content on microstructure and shape-memory properties of Ti–Ni–Pd–Cu alloys. *Mater Sci Eng A* 602:19–24
20. Khan MI, Kim HY, Miyazaki S (2015) A review of TiNiPdCu alloy system for high temperature shape memory applications. *Shape Mem Superelast* 1:85–106
21. Lin K, Wu S-K, Wu L-M (2009) Martensitic transformation of cold-rolled and annealed $\text{Ti}_{50}\text{Ni}_{40}\text{Cu}_{10}$ shape memory alloy. *Mater Trans* 50:2384–2390